ARMY RESEARCH LABORATORY

Modeling of Acoustic Pressure Waves in Level-Dependent Earplugs

by James DeSpirito and Mary S. Binseel

ARL-TR-4607   **September 2008**

NOTICES

Disclaimers

Army Research Laboratory

Aberdeen Proving Ground, MD 21005-5066

ARL-TR-4607   **September 2008**

Modeling of Acoustic Pressure Waves in Level-Dependent Earplugs

James DeSpirito
Weapons and Materials Research Directorate, ARL

Mary S. Binseel
Human Research and Engineering Directorate, ARL

1. REPORT DATE *(DD-MM-YYYY)*	2. REPORT TYPE		3. DATES COVERED (From - To)
September 2008	Final		October 2006–December 2007

4. TITLE AND SUBTITLE	5a. CONTRACT NUMBER
Modeling of Acoustic Pressure Waves in Level-Dependent Earplugs	
	5b. GRANT NUMBER
	5c. PROGRAM ELEMENT NUMBER

6. AUTHOR(S)	5d. PROJECT NUMBER
James DeSpirito and Mary Binseel	622105AH84
	5e. TASK NUMBER
	5f. WORK UNIT NUMBER

7. PERFORMING ORGANIZATION NAME(S) AND ADDRESS(ES)	8. PERFORMING ORGANIZATION REPORT NUMBER
U.S. Army Research Laboratory ATTN: AMSRD-ARL-WM-BC Aberdeen Proving Ground, MD 21005-5066	ARL-TR-4607

9. SPONSORING/MONITORING AGENCY NAME(S) AND ADDRESS(ES)	10. SPONSOR/MONITOR'S ACRONYM(S)
	11. SPONSOR/MONITOR'S REPORT NUMBER(S)

12. DISTRIBUTION/AVAILABILITY STATEMENT
Approved for public release; distribution unlimited.

13. SUPPLEMENTARY NOTES

14. ABSTRACT
The report describes both experimental and computational fluid dynamic (CFD) characterizations of acoustic pressure wave travel through a level-dependent hearing protection device, or earplug. The Army's Combat Arms Earplug (CAE) was the device evaluated. Experimental real-ear attenuation at threshold measurements compared very well with design specifications for the CAE. Experimental continuous noise measurements showed higher than desired attenuation in the 1- to 4-kHz range. Experimental impulse tests provided dynamic response data under field-type conditions and were used to validate the CFD predictions. CFD predictions of the continuous noise input underpredicted the attenuation at higher frequencies. Predicted values of impulse noise attenuation were good, to within 15% of the experimental values.

15. SUBJECT TERMS
acoustics, level-dependent earplugs, muffler, computational fluid dynamics, real-ear attenuation at threshold

16. SECURITY CLASSIFICATION OF:			17. LIMITATION OF ABSTRACT	18. NUMBER OF PAGES	19a. NAME OF RESPONSIBLE PERSON James DeSpirito
a. REPORT	b. ABSTRACT	c. THIS PAGE			19b. TELEPHONE NUMBER *(Include area code)*
UNCLASSIFIED	UNCLASSIFIED	UNCLASSIFIED	UL	32	(410) 306-0778

Contents

List of Figures

List of Tables

Acknowledgments

INTENTIONALLY LEFT BLANK.

1. Introduction

Soldiers rely heavily on their hearing in combat environments to maintain their situational awareness. In many situations, hearing a sound is their first cue to events of importance to their survival and mission accomplishment. They also must communicate, both over radios and face-to-face. Finally, their hearing must be protected so that they may continue these tasks and not become a combat casualty. A single impulse sound (such as a weapon firing) may be sufficient to cause temporary or permanent hearing loss. Listening, communicating, and protecting hearing are often conflicting requirements, as many hearing protection devices (HPDs) do a good job preserving hearing but at the cost of blocking sounds the Soldier needs to hear. A potential solution for protecting hearing in military environments is the use of level-dependent (also called nonlinear) HPDs. These HPDs allow low, nondamaging level sounds to pass through relatively unimpeded (allowing environmental monitoring and communications), yet at high, impulsive noise levels additional attenuation is activated due to the design of various elements in the earplug, thus protecting hearing. The Army's Combat Arms Earplug (CAE) (figure 1) is one example of such a device.

Figure 1. Combat Arms Earplug.

The CAE is a double-sided earplug. The dark green side is a standard triple-flange earplug with a solid stem. This side would be inserted in high continuous noise environments, such as when riding in an armored vehicle. The yellow side is nonlinear and is used where the continuous noise levels are not damaging, but impulse sounds may occur, such as in dismounted operations. The stem of this side contains an auditory pathway within which are structures (chambers and orifices) that attenuate impulsive sounds. The entrance to the pathway is shown circled in figure 1.

The CAE functions well; however, feedback from Operation Iraqi Freedom indicates that Soldiers and Marines would like less attenuation of lower-amplitude sounds. Their perception is that too much attenuation occurs at these low levels, interfering with their ability to hear. Hence,

there is a need for an earplug that has very low passive attenuation in the auditory pass band yet provides protection from sudden high-amplitude acoustic waves.

Modifying the CAE's or similar earplug's parameters (orifice size and number, for example) could yield an earplug with the desired frequency and amplitude response characteristics. In order to search efficiently for an optimal solution and have a good theoretical basis for manipulating the parameters, the passage of acoustic waves should be modeled through elements similar to those found in these devices. By this modeling, understanding may be gained about how various elements (chambers, orifices, filters, baffles, and diaphragms, for example) modulate the energy that is passed through to the wearer and explore earplugs that would address Soldiers' concerns without degrading the hearing protection provided by the earplugs.

The objective of this effort was to develop a validated computational fluid dynamic (CFD) model of acoustic pressure wave travel through level-dependent hearing protectors. Such a model could eventually be used to assess current level-dependent earplug elements and to predict the sound attenuation characteristics of conceptual elements. Although there is some work in the literature on using CFD to model larger acoustic elements, such as mufflers, modeling of such small acoustic elements is a unique effort.

2. Approach

The implementation goal of this research is to develop level-dependent hearing protection with properties customized for particular applications. By developing a robust CFD model of earplug elements, changes can be virtually evaluated for their earplug performance impacts. This will enable research in nonlinear elements by eliminating the need for physical prototypes of unpromising configurations. The approach included developing the CFD model and validating it initially for the CAE by comparing predictions from the model to measured earplug characteristics. This work was a joint effort between the U.S. Army Research Laboratory (ARL) Weapons and Materials Research Directorate (WMRD) and Human Research and Engineering Directorate (HRED). HRED was responsible for providing experimental characterization of the attenuation of the CAE under both continuous and impulse noise conditions. WMRD was responsible for numerically modeling the CAE internal geometry using their CFD capabilities and resources, including the ARL Major Shared Resource Center's (MSRC's) high-performance computing facilities. The following approach description is divided into experimental and computational sections.

2.1 Experimental

The following experimental measurements were made to provide physical data for validation of CAE CFD modeling. These measurements included attenuation of impulse noise, attenuation of continuous noise, and real-ear attenuation at threshold (REAT).

2.1.1 Impulse Measurements

The attenuation of the pressure wave that travels though the CAE (nonlinear side) during exposure to an impulse noise was measured at HRED's M Range (an instrumented small-arms range). The impulse events were created using an M4 rifle, a shortened variant of the M16A2. Figure 2 shows a typical test setup.

The earplugs were inserted into a special impulse manikin built by the French-German Research Institute of Saint-Louis (ISL). The ISL manikin (or "head") is specifically built to withstand high-impulse sound environments without excitation of the microphones from pathways other than that of the ear and ear canal. The ISL head consists of a headform with artificial ears and is instrumented with two Brüel & Kjær (B&K) model 4136 microphones placed at the site where the tympanic membranes (eardrums) would be located in a human. The microphones were polarized with 28 V.

(a)   (b)
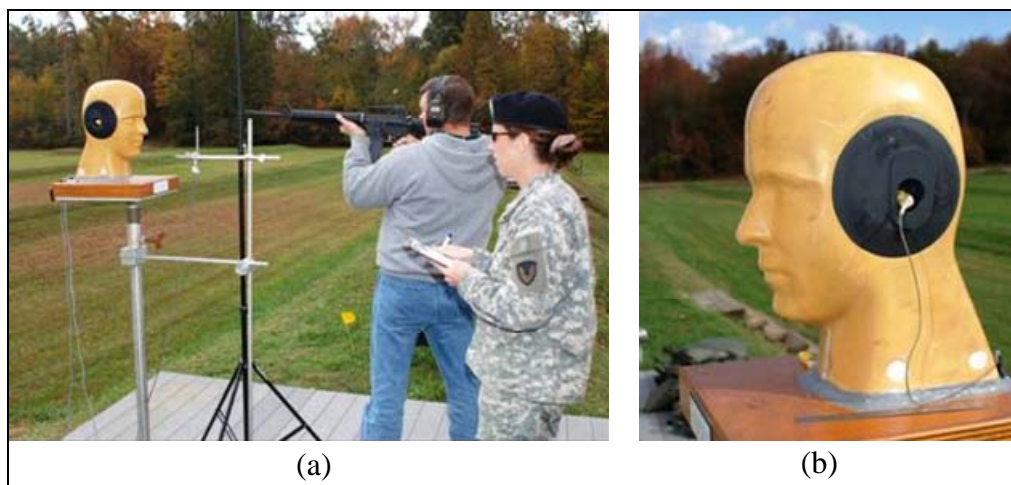
Figure 2. Typical impulse measurement setup (a) and ISL impulse manikin (b).

A third B&K 4136 microphone with a polarization of 28 V was used to measure the free-field sound. This microphone was placed close to and in the plane of the manikin head at a grazing angle to the sound source used.

Various peak pressure levels at the head were created by firing the M4 rifle at varying distances from the manikin. Distances of 0.25, 0.5, 1, 2, 4, 8, 16, 32, and 64 m were used, resulting in free-field peak pressure levels at the manikin location that varied from a low of 125-dB (20-μPa reference pressure) peak at 64 m to a high of about 187-dB peak at 0.25 m. The output of the

microphones was processed through a Tucker-Davis Technologies TDT2 AP2 array processor and stored on a portable computer. At the two farthest distances (32 and 64 m), the shooter stood on a stepladder in order to prevent multipath pressure waves from overlapping the primary impulse signal. Results of the impulse noise measurements are listed in table 1. The difference between the ISL ear peak pressure with the CAE inserted and the corresponding free-field peak pressure is the peak pressure reduction. Free-field measurements of the peak pressure and the measurements at the manikin microphone are shown.

Table 1. Impulse noise measurement results (in peak decibel, dB P,
p_{ref} = 20 µPa).

Distance (m)	Free Field (dB P)	CAE (dB P)	Peak Pressure Reduction (dB)
0.25	186.91	156.48	30.43
0.5	180.61	153.01	27.60
1	172.06	145.29	26.76
2	164.05	141.30	22.75
4	155.66	136.09	19.57
8	148.15	131.21	16.94
16	139.76	125.52	14.24
32	134.84	123.76	11.08
64	125.48	113.54	11.94

2.1.2 Continuous Noise Attenuation

CAE attenuation measurements were taken in the REAT chamber in the HRED Environmental Laboratory (Room 21, Bldg. 520, Aberdeen Proving Ground). The earplugs were inserted in a Knowles Electronics Manikin for Acoustic Research (KEMAR), shown in figure 3.[*] KEMAR, like the ISL head, is instrumented with microphones placed at the location of a person's eardrums. Berger (*1*) includes a discussion of these types of test fixtures and the various methods for measuring hearing protector attenuation. Although KEMAR can be too acoustically leaky for these types of measurements, for earplugs with an intentional acoustic pathway, such as the CAE, KEMAR is an acceptable test fixture (*2*).

Pink noise (noise with equal energy in all octave bands) was used as an input signal for the continuous attenuation measurements. The pink noise was presented in a reverberant room through a trio of Electro-Voice S_x500+ loudspeakers amplified by two Crown Macro-Tech 602 amplifiers. The loudspeakers were positioned such that a diffuse sound field was generated within a sphere of ~1 m at the center of the room, where the KEMAR was positioned. The sound level was measured in A-weighted decibels (dB A) using a CEL Instruments model

---

[*]The ISL head was not appropriate for continuous noise measurements because its microphones are designed for high-level sounds and do not function at the lower levels used in the continuous noise measurements. Conversely, KEMAR cannot be used for impulse measurements because its microphones are unsuitable for the very high-impulse sound levels.
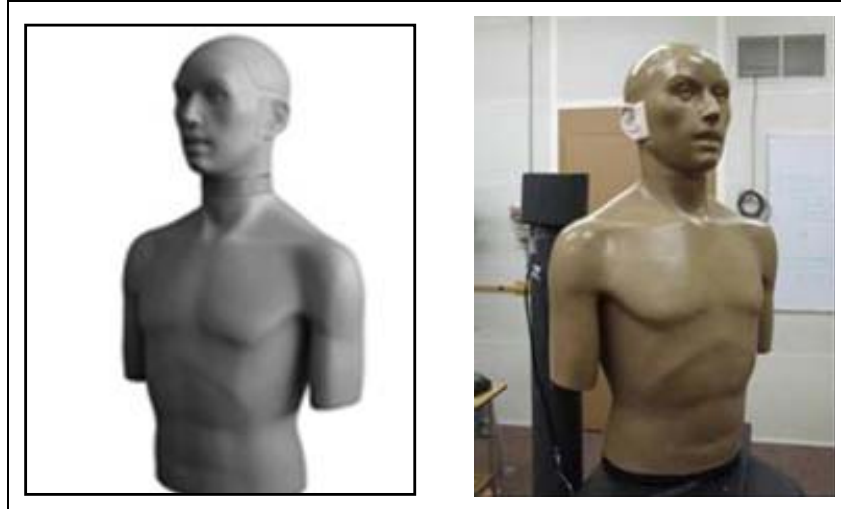
4

Figure 3. Knowles Electronics Manikin for Acoustic Research (KEMAR).

573.C1 sound level meter. Sound pressure levels (SPLs) of 45, 65, 85, and 100 dB A ($p_{ref} = 20$ µPa) were used. Recordings were then made through the KEMAR with and without the CAE inserted. Unoccluded (no earplug) measurements were taken once. Three measurements were taken with CAE inserted into the KEMAR ear canals with removal and reinsertion of the earplugs between measurements. Measurements were made with linear weighting. Results of the continuous noise measurements for the three highest SPLs are listed in table 2.

2.1.3 Real-Ear Attenuation Measurements

REAT is a method for obtaining attenuation measurements of HPDs using human participants. The methodology is described in an American National Standards Institute (ANSI) standard (*3*). The measurements were performed under protocol ARL 20098-07026, and the investigators have adhered to the policies for protection of human subjects as prescribed in AR 70-25. The REAT methodology is to obtain two sets of auditory threshold measurements using one-third octave narrow band noise at seven center frequencies (125, 250, 500, 1000, 2000, 4000, and 8000 Hz). One set of thresholds is obtained with the hearing protector in place, and the other is obtained with it removed. The difference in the two sets of thresholds is the attenuation of the hearing protector. Each paired set of measurements (one without and one with the earplug in place) constitutes one trial. Each of the 10 participants performed two trials. The results of the trials are used as described in ANSI S12.6-1997 (*3*) to calculate the attenuation of the earplugs at the seven center frequencies.

The REAT measurements were performed in the same reverberant room and used the same amplifiers and loudspeakers to deliver the stimuli as in the continuous noise measurements. The REAT signals were generated by an Interacoustics AC40 clinical audiometer. Results of the REAT measurements are listed in table 3.

Table 2. Continuous noise measurement results.

Hz	100 dB			85 dB			65 dB		
	CAE	Unoccl.	Atten.	CAE	Unoccl.	Atten.	CAE	Unoccl.	Atten.
63	69.7	70.2	0.5	55.3	56.6	1.3	22.9	34.6	11.7
80	65.6	66.8	1.2	48.7	51.8	3.1	20.4	29.7	9.3
100	70.0	70.8	0.8	51.7	55.6	3.9	21.9	24.4	2.5
123	79.9	80.8	0.9	64.6	67.1	2.5	31.2	34.6	3.4
160	85.6	86.5	0.9	71.8	73.4	1.6	41.0	44.0	3.0
200	81.5	83.0	1.5	70.8	70.5	–0.3	45.2	45.3	0.1
250	87.0	89.5	2.5	75.7	77.0	1.3	49.6	53.1	3.5
315	84.2	88.5	4.3	70.9	76.6	5.7	49.7	57.7	8.0
400	84.6	91.8	7.2	73.6	79.8	6.2	54.9	60.7	5.8
500	81.7	91.7	10.0	70.6	80.2	9.6	53.3	62.0	8.7
630	78.5	92.9	14.4	66.9	81.1	14.2	48.8	62.0	13.2
800	72.6	90.0	17.4	61.3	78.2	16.9	42.7	58.9	16.2
1000	65.2	85.8	20.6	55.1	73.8	18.7	36.3	54.3	18.0
1250	63.1	86.4	23.3	54.7	74.6	19.9	35.9	55.1	19.2
1600	63.2	90.8	27.6	54.4	79.1	24.7	35.4	59.7	24.3
2000	63.9	96.5	32.6	52.8	84.5	31.7	32.7	64.8	32.1
2500	62.6	97.3	34.7	51.2	85.4	34.2	31.8	65.9	34.1
3150	62.9	92.1	29.2	51.5	80.2	28.7	33.0	60.6	27.6
4000	64.8	87.7	22.9	52.8	75.8	23.0	32.7	56.1	23.4
5000	73.7	89.6	15.9	60.6	77.4	16.8	38.0	57.8	19.8
6300	79.7	94.5	14.8	67.7	82.2	14.5	46.7	62.2	15.5
8000	78.4	94.5	16.1	66.1	82.4	16.3	50.0	62.4	12.4

Table 3. Real-ear attenuation at threshold values for the CAE nonlinear side.

		Frequency (Hz)						
		125	250	500	1000	2000	4000	8000
Attenuation (dB)	Mean	3.00	3.25	7.75	13.00	19.75	21.25	18.50
$p_{ref} = 20\ \mu Pa$	Std. dev.	3.07	3.55	2.49	7.34	5.20	4.60	3.76

2.2 CFD Modeling

As stated previously, the CAE (figure 1) is a dual-purpose device. When the green side is in the ear, the CAE operates like a standard HPD to be used for exposure to steady, high-level noise (aircraft, armored vehicles, etc.). When the yellow side is in the ear, the CAE operates as a level-dependent device, which allows "hear-through" protection at ambient noise levels while attenuating impulse noise (e.g., gunshots). The active feature of the CAE is the acoustic element (the white plastic part in figure 1, which is shown as a solid model in figure 4).
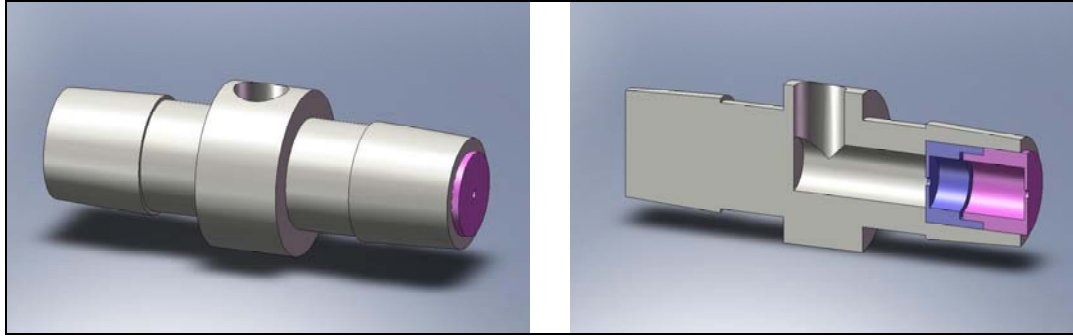
Figure 4. Full and cutaway solid model views of CAE acoustic element.

The green side contains the solid section of the acoustic element, so it acts as a standard HPD when inserted. The yellow flanged component contains a passage that extends from the acoustic element so that sound is transmitted from outside the CAE. However, an acoustic filter (the blue and pink parts in figure 4) attenuates the impulse noise signals.

The internal passageway, including the acoustic filter, was modeled using a three-dimensional, unstructured mesh of both hexahedral and tetrahedral cells. It was found that an "extension" chamber past the exit of the filter was needed to obtain downstream pressure levels. The extension chamber was 8 mm long, about one-half the length of the passage in the yellow flange. The size of the computational mesh (figure 5) was about 2.3 million cells and took advantage of half-plane symmetry. The mesh size was driven by the need for near-uniform cell sizes and to resolve the very small orifices of the acoustic filter (about 0.13 mm). A mesh independence investigation using both coarser and finer meshes confirmed that this mesh was appropriate.
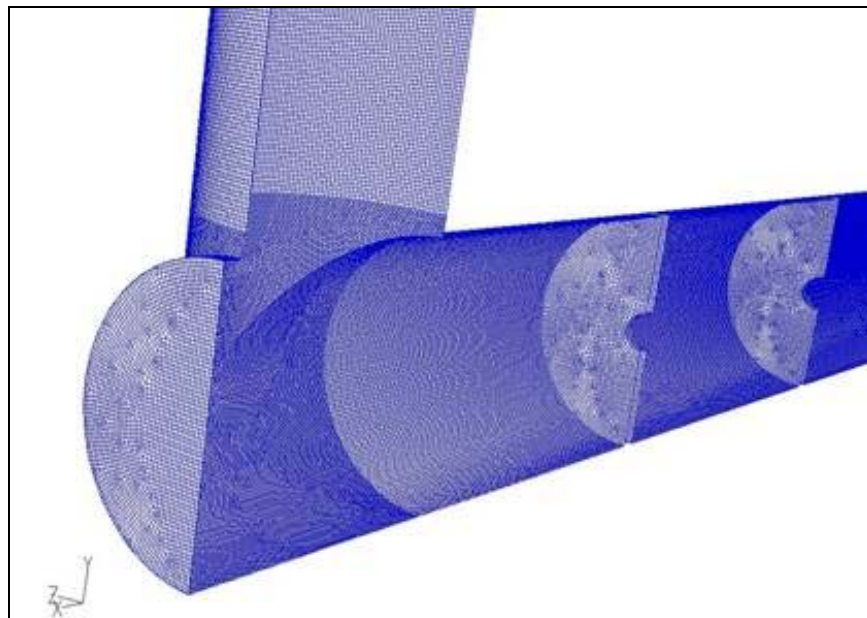

Figure 5. Computational mesh of CAE acoustic element and extension chamber.

Similarly, the size of computational time step was driven by the need to resolve wave travel through the small cavities of the CAE. A time step of 5.0×10^{-7} s was used in all calculations except the two shortest distance impulse simulations, which required a time step of 2.5×10^{-7} s to resolve the sharp rise to the high-peak input impulse pressure at those distances. The former time step corresponds to a Nyquist frequency of 1 MHz, which is much higher than is required to resolve the 20-kHz maximum frequency of interest in auditory acoustics (*4*).

The commercial CFD code FLUENT (*5*) was used in this study. FLUENT is a general-purpose CFD package that supports flows that range from incompressible through hypersonic; single- and multiphase flows; and most state-of-the-art turbulence modeling capabilities for both Reynolds-averaged Navier-Stokes (RANS) and hybrid RANS and Large-Eddy Simulation methodologies. In these simulations, the pressure-based solver was used with the noniterative transient analysis (NITA), a second-order, implicit approach that eliminates the need for subiterations at each time step. The PISO (pressure-implicit splitting of operators) scheme was used for pressure-velocity coupling and spatial discretization was second order for the pressure equation and third-order MUSCL (monotone upstream-centered schemes for conservation laws) for the density, momentum, and energy equations. All simulations were run with the laminar flow option.

Some computations were performed on local Dell Linux workstations, each with two dual-core 2.66-GHz Intel Xeon processors. The larger-scale simulations were run on the ARL MSRC Linux Network machine that has 2048, 3.6-GHz Intel Xeon EM64T processors. The largest simulations used 32 machine processors.

The pressure history was recorded at the 10 locations shown in figure 6. The pressure input was recorded at P1. The exit of the CAE acoustic filter is at P4. Locations P5–P9 are on the chamber wall at 1, 2, 4, 6, and 8 mm from the filter exit. The outlet of the computational domain was as P10. Data from locations P5–P8 were used for the impulse simulations while data from location P6 were used for the continuous noise simulations.
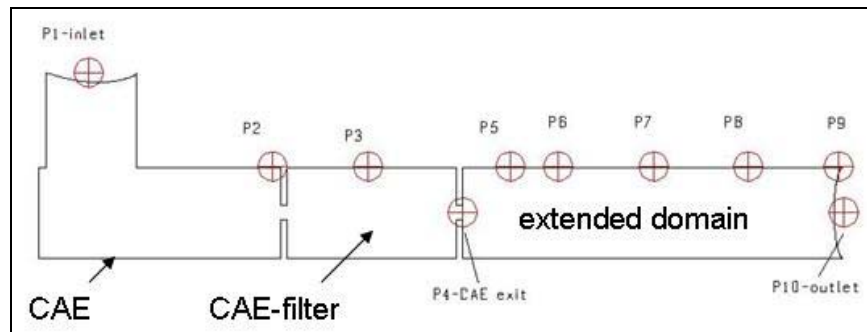

Figure 6. Locations of pressure history probes.

The input signal was applied uniformly across the inlet boundary. The continuous noise input was simulated using numerically generated white noise at nominal SPLs of 45, 65, 85, and 100 dB. For the impulse simulations, the actual free-field pressure from the experiment was input at the inlet boundary. Both of these boundary conditions were applied using user-defined functions (UDFs), which are user-written C-code that allows direct access to the FLUENT solver.

3. Results

3.1 Preliminary Studies

Several basic validation cases were first performed to demonstrate that RANS simulations are adequate to predict the response of basic acoustic elements. Acoustic simulations were performed in a straight duct, an expansion chamber (low-pass filter), a vented duct (high-pass filter), and a duct with a Helmholtz cavity (band-pass filter). The geometry and setup of these simulations were based on an acoustic filter description by Professor D. A. Russell, from Kettering University (6). Figure 7 shows the cases investigated in this preliminary study. The straight duct and expansion chamber were modeled using axisymmetry. Three-dimensional meshes were required for the side branch and Helmholtz resonator cases, but center-plane symmetry was used to reduce the mesh size by one-half.

The procedure for the simulation of each duct case was the same. The pressure-based NITA solver was used to perform a transient computation (2.5×10^{-4} s time step) to calculate the pressure response at the output of the duct due to a given input pressure. The input pressure consisted of a white Gaussian noise signal, generated using the following equation (4):

$$P = (-2 \ln R_1)^{\frac{1}{2}} \cos(2\pi R_2) \ , \tag{1}$$

where P is the pressure and R_1 and R_2 are random numbers. P will be normally distributed with a mean of zero and a standard deviation of one. P can be given an arbitrary mean and standard deviation by taking the number generated by equation 1, multiplying it by the desired standard deviation, and adding the desired mean. Equation 1 was implemented in a UDF in FLUENT that applied the correct pressure at the input boundary at each time step. The outflow boundary was modeled with a pressure output boundary condition with a static pressure and temperature of 101 kPa and 300° K, respectively. The wall boundary was modeled via a no-slip condition and laminar flow was assumed. The axial and radial mesh spacing was 0.25 and 0.2 cm, respectively.
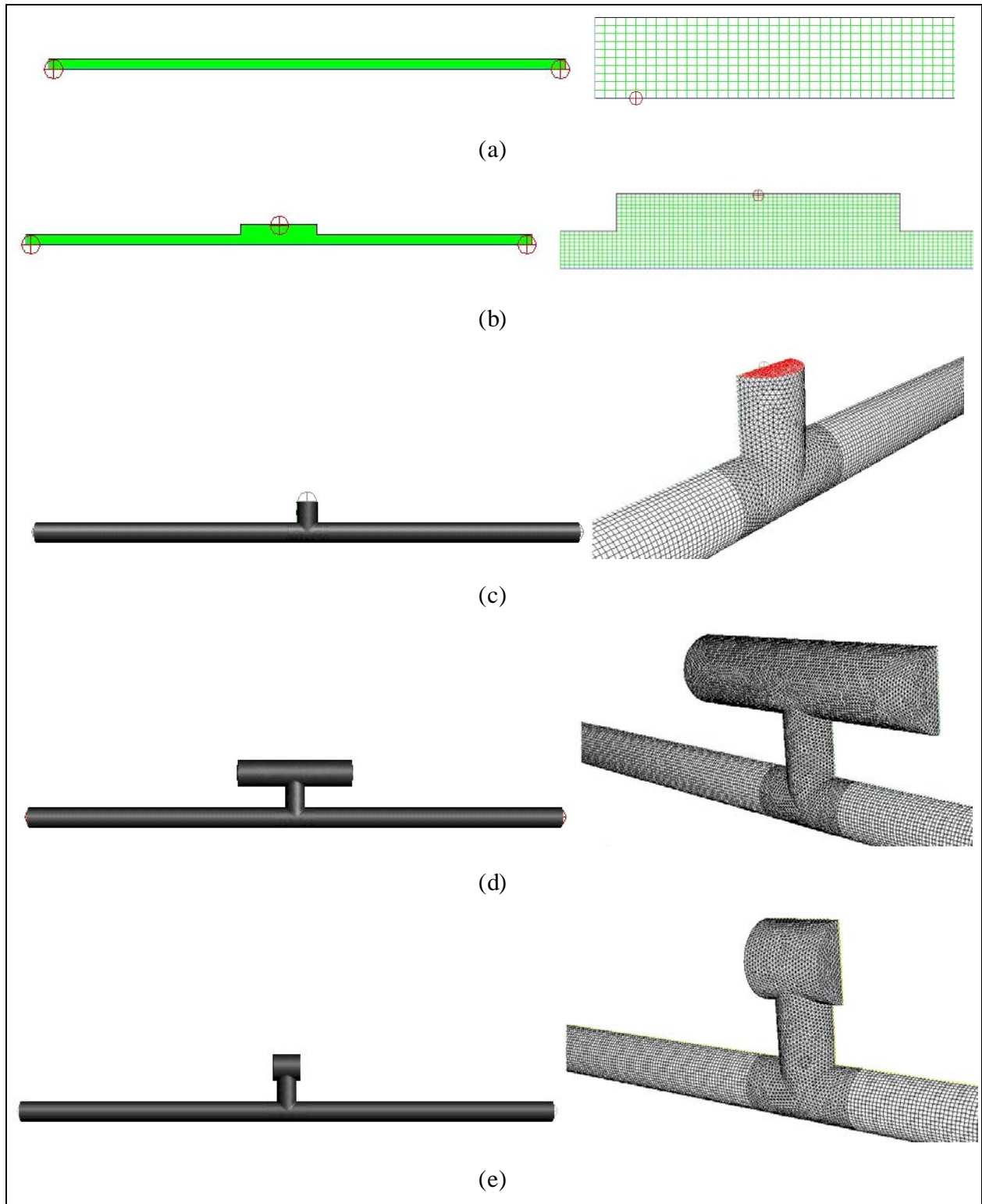
Figure 7. Acoustic elements: (a) straight duct, (b) expansion chamber (low-pass filter), (c) duct with side branch (high-pass filter) and Helmholtz resonator (band-pass filter) designed for (d) 166 Hz and (e) 333 Hz.

3.1.1 Open Duct

Each duct in these preliminary studies has a length, L, of 101 cm and a diameter of 3.9 cm. The resonant frequencies for an unflanged, open duct can be approximated by (*6*)

$$f_n = \frac{nc}{2(L + 0.61a)},$$ (2)

where $n = 1,2,3,\dots$, a is the duct radius, c is speed of sound, and the length of the duct includes an "end correction," $L_{eff} = (L + 0.61a)$. The fundamental and first harmonic frequencies for this duct are $f_1 = 170$ and $f_2 = 340$ Hz.

The input signal at the left end was generated by equation 1 using a standard deviation of 20, resulting in an SPL of about 90 dB (figure 8a). The output signal is shown in figure 8b–c in the form of SPL, the transmission coefficient (TC), and the transmission loss (TL), where

$$TC = 20\log_{10}\left(\frac{P_{out}}{P_{in}}\right)$$ (3)

and

$$TL = 20\log_{10}\left(\frac{P_{in}}{P_{out}}\right).$$ (4)

Figure 8 shows that the first two frequencies were captured in the simulation, with the third nearly visible. The calculated fundamental frequency was 168 Hz, very close to that from equation 2. The second frequency was 316 Hz, vs. 340 Hz from equation 2. The CFD predicts the resonant frequencies of the open duct reasonably well, to within 1% and 7% for the first and second modes, respectively.

3.1.2 Expansion Chamber (Low-Pass Filter)

The diameter of the expansion chamber, figure 7b, is twice that of the duct, and the length is 15 cm. Figure 9 shows the calculated transmission loss (equation 4) for the expansion chamber compared to the unfiltered duct response. The calculated fundamental frequency for the expansion chamber is 121 Hz, and the second frequency is calculated as 344 Hz. Since it acts as a low-pass filter, the response of the expansion chamber is observed to be attenuated (higher transmission loss) at frequencies above the fundamental.
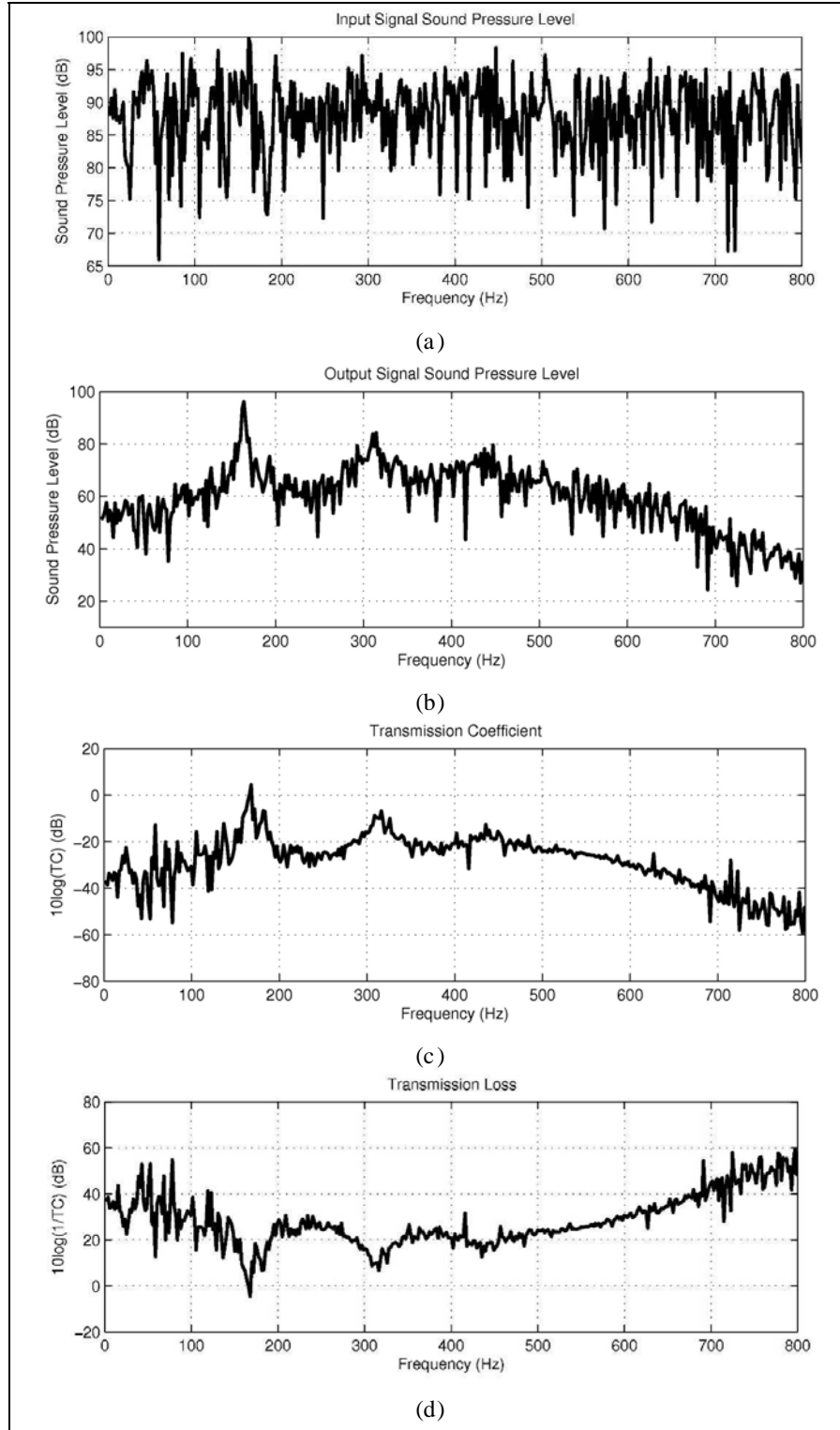
Figure 8. Input and output signals in straight duct simulation: (a) input SPL, (b) output SPL, (c) transmission coefficient, and (d) transmission loss.
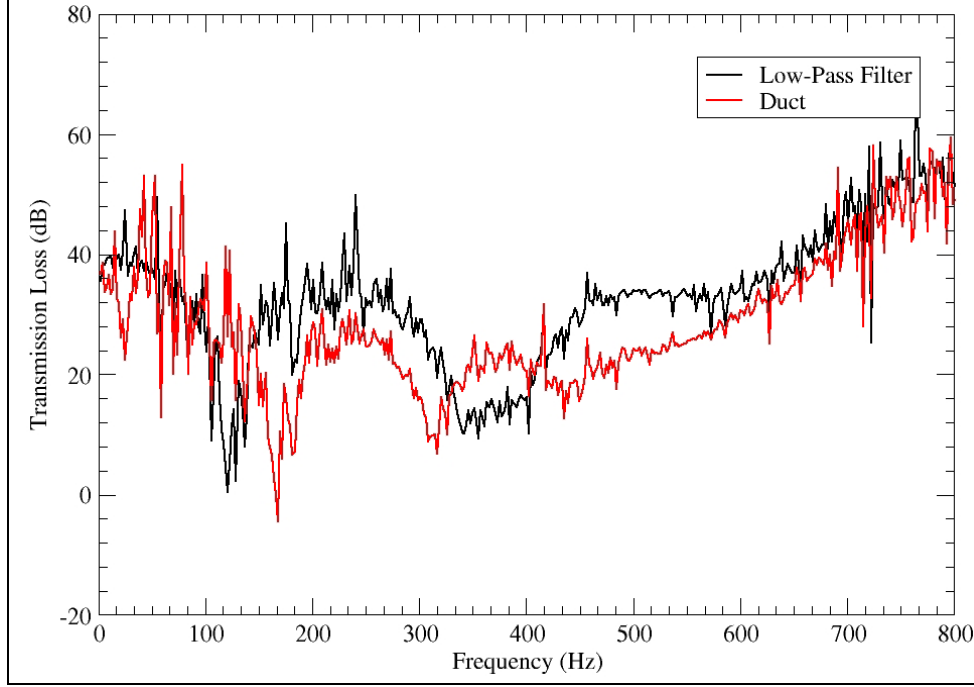
Figure 9. Transmission loss calculated in expansion chamber (low-pass filter) simulation.

3.1.3 Duct With Side Branch (High-Pass Filter)

The diameter and length of the side branch are each 3.9 cm. Figure 10 shows the calculated transmission loss for the duct with a side branch compared to the unfiltered duct response. Since the side branch acts as a high-pass filter, the calculated fundamental frequency is now 283 Hz, with the fundamental frequency of the unfiltered duct completely attenuated. The response at the higher frequencies (>500 Hz) is the same as the unfiltered duct.

3.1.4 Helmholtz Resonator (Band-Pass Filter)

A Helmholtz resonator acts much like a simple mass-spring system, having both inertia and compliance. The cavity resonates at a frequency

$$\omega_0 = c\sqrt{\frac{S_b}{L_{eff}V}} , \tag{5}$$

where S_b is the neck area, $L_{eff} = L + 1.7a$ is an effective neck length, and V is the cavity volume.

In the process of resonating, the cavity will absorb energy at the design frequency. All the absorbed energy is returned to the pipe later in the cycle, but due to phase relationships, it is returned toward the source, not toward the outlet. The resonator acts as a filter that will "pass" all the frequencies outside the design bandwidth. It is also (perhaps more aptly) called a "band-stop" filter because it will stop all the frequencies inside the design bandwidth.
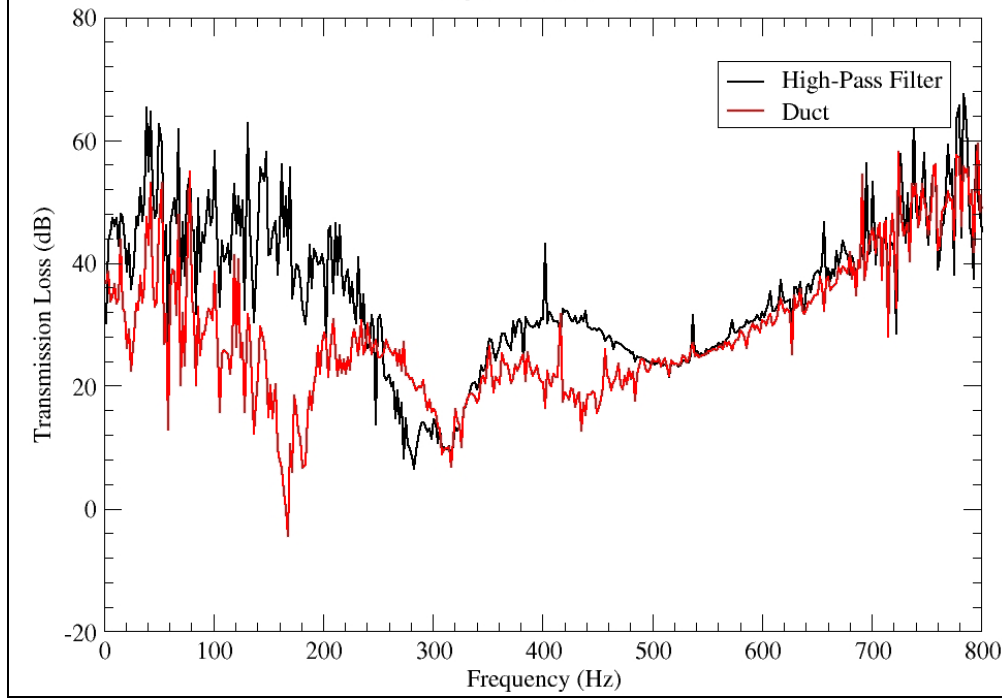
13

Figure 10. Transmission loss calculated in duct with side branch (high-pass filter) simulation.

Two design frequencies were chosen for this preliminary study, 166 and 333 Hz. For each case the length of the neck, L, was 3.9 cm and the diameter of the cavity was 5.08 cm. The length of the cavity was 21.7 cm for the lower-frequency case and 5.4 cm for the higher-frequency case. Figure 11 shows the calculated transmission loss for the two Helmholtz resonators, compared to the unfiltered duct response and the theoretical transmission loss (*6*),

$$TL = 10\log_{10}\left[1+\left(\frac{c^2}{4S^2\left(\dfrac{\omega L_{eff}}{S_b} - \dfrac{c^2}{\omega V}\right)^2}\right)\right].$$
(6)

When $\omega = \omega_0$, the resonance frequency of the resonator, the transmitted power is zero and the transmission loss is a maximum.

For the 166-Hz resonator (figure 11a), the calculated transmission loss shows that the frequencies are attenuated near the design frequency. The fundamental response frequency has moved down to 116 Hz. The second response frequency is 317 Hz, very close to that of the unfiltered duct (316 Hz). Compared to the unfiltered duct, there was some additional attenuation of the response in the frequency range 200–500 Hz.

14
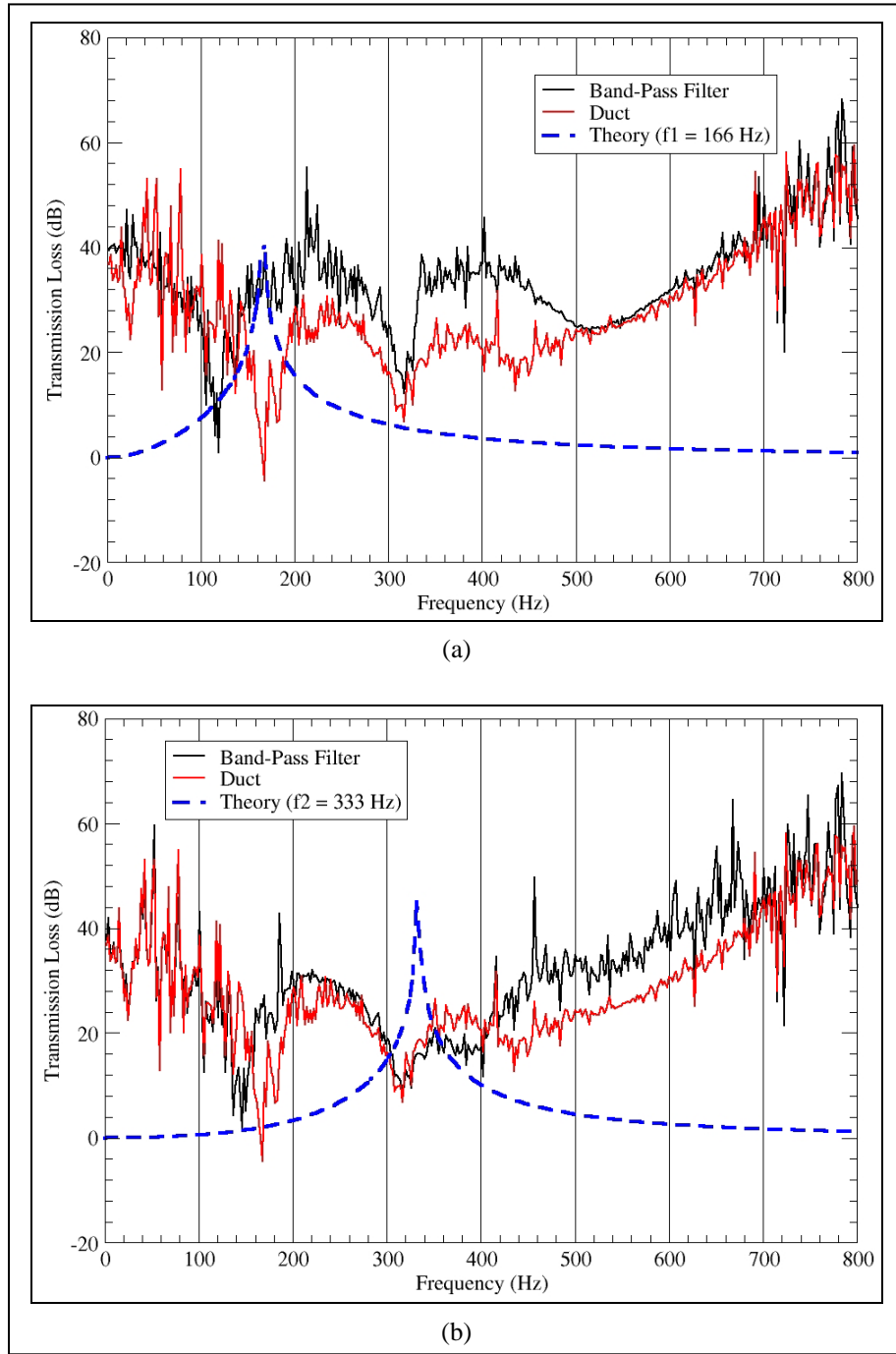
Figure 11. Transmission loss calculated in duct with Helmholtz resonator (band-pass filter) simulation: (a) design frequency f_1 and (b) design frequency f_2.

The result for the 333-Hz resonator (figure 11b) is not as good, with no attenuation observed near the design frequency. The frequency and transmission loss of the second frequency is the same as the unfiltered duct, 316 Hz. It is likely that the second cavity is not sized properly to act as a Helmholtz resonator. The ratio of the cavity volume to neck volume was only 1.4 for the

smaller cavity, as opposed to 5.6 for the larger cavity. Additionally, the neck diameter is similar to the characteristic dimensions of the cavity. The higher-frequency cavity should have been designed with a smaller neck area.

3.1.5 Expansion Chamber Muffler

Another validation simulation modeled the acoustic performance of a simple expansion chamber muffler (7, 8). Figure 12 compares the predicted transmission loss (equation 4) to experimental data (7, 8) and to one-dimensional (1-D) theory, which is computed from equation 7 (6, 9):

$$TL = 10\log_{10}\left(\cos^2(kL_2) + 0.25\left(\frac{S_2}{S_1} + \frac{S_1}{S_2}\right)^2 \sin^2(kL_2)\right). \tag{7}$$

Here, S_1 and S_2 are the areas of the duct and expansion chamber, respectively; k is the wave number; and L_2 is the length of the expansion chamber. The predicted values compare very well to the experimental data across the given frequency range. Both the CFD predictions and the experimental data diverge from the 1-D theory at about 1500 Hz, indicating the breakdown of the simplified theory above this frequency.
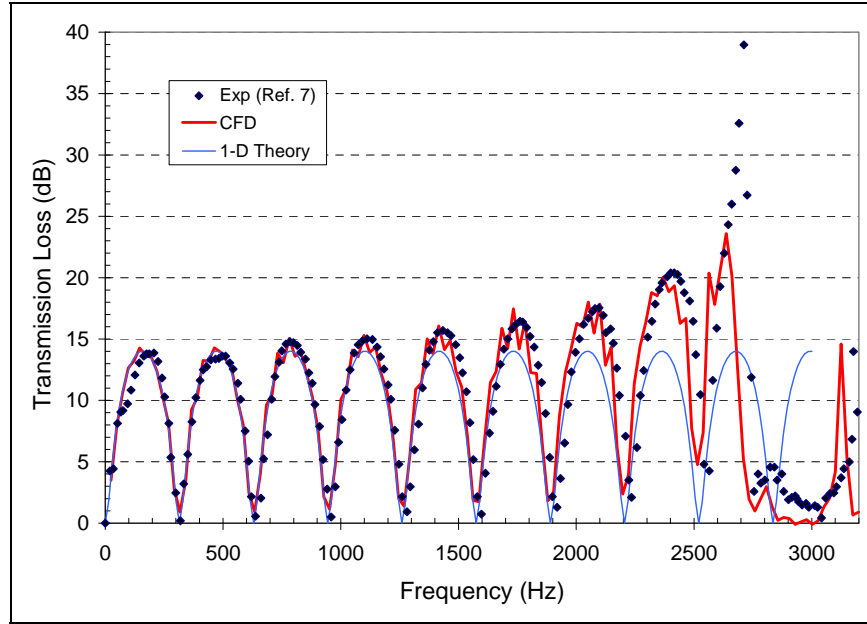

Figure 12. Comparison of predicted transmission loss with 1-D theory.

As a result of these preliminary studies, a level of confidence was achieved that the response of the CAE could be predicted using this CFD methodology.

3.2 CAE Investigation

Computations of the continuous noise cases showed that the attenuation at all four SPL levels investigated was similar. Therefore, the results for only one case are shown in figure 13, which compares the CFD-predicted SPL to the HRED experimental data at an input SPL of 65 dB. The CFD computations overpredict the attenuation at lower frequency and underpredict attenuation at higher frequency. Part of this may be due to the different input noise used in the CFD vs. the experiment, which used pink noise for the input. Pink noise should have also been used in the CFD; however, white noise was used. White noise contains equal energy at all frequencies, therefore more energy was contained in the higher-frequency bands for the input to the CFD simulations. The shapes of the curves compare very well at frequencies above 1000 Hz.
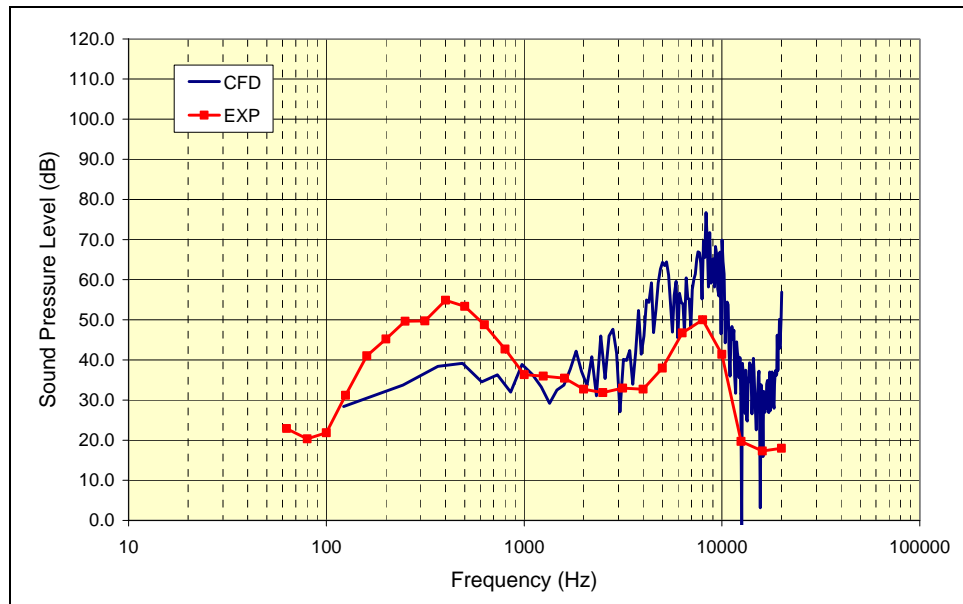

Figure 13. Sound pressure level, 65-dB continuous noise input.

These same data are plotted in figure 14 in the form of TL. Also plotted is the HRED experimental REAT data and the data (assumed REAT) from the CAE E-A-R design specifications sheet (*10*). The REAT values are actually insertion loss (IL, the difference between SPL at the same reference point without and with HPD in place) rather than transmission loss (equation 1), so direct comparison to the CFD and continuous noise experiment values may be dubious. However, it does show that the HRED REAT data compared very well to the CAE specifications (the blue and brown curves, respectively, in figure 14). Interestingly, the experimental continuous noise attenuation level in the frequency range of 1 to 4 kHz is very close to the attenuation level provided by the green (standard HPD) side of the CAE (the red and green curves, respectively). This may indicate the frequency range where there is an opportunity to improve the current earplug's level-dependent acoustic element.
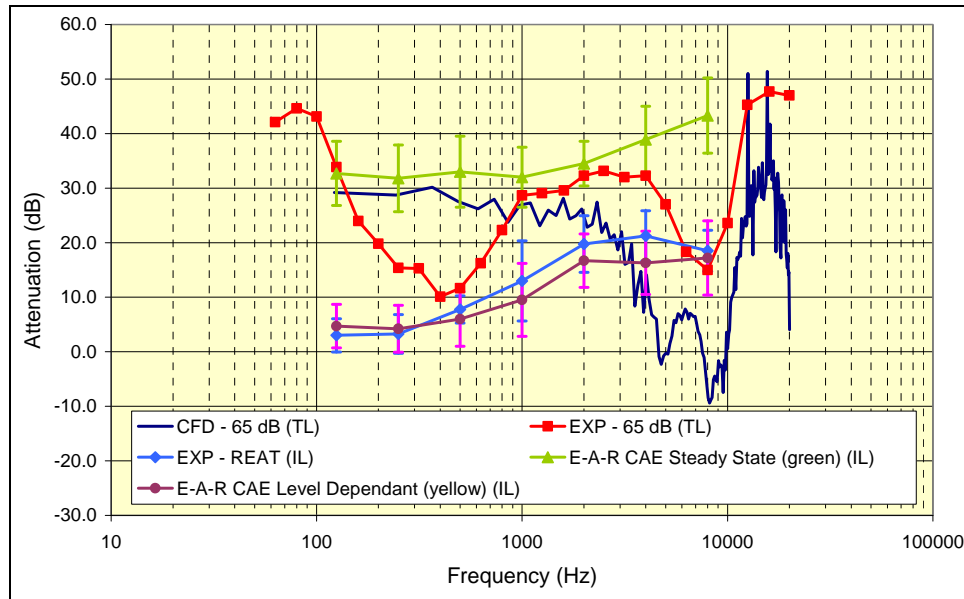
17

Figure 14. Transmission loss (continuous noise case) and insertion loss (REAT) values.

The CFD predictions for the nonlinear impulse response were better than the continuous noise results. Figure 15 shows the impulse input results plotted as the reduction in peak pressure between the impulse pressure and the response pressure measured in the ear canal. The CFD result was somewhat dependent on the location used for the receiving probe location. The values from probe locations P5–P8 were averaged, and the minimum and maximum values at those four locations were used to generate the error bars. Over most of the distance range, the maximum difference between the CFD and experimental values is about 15%.
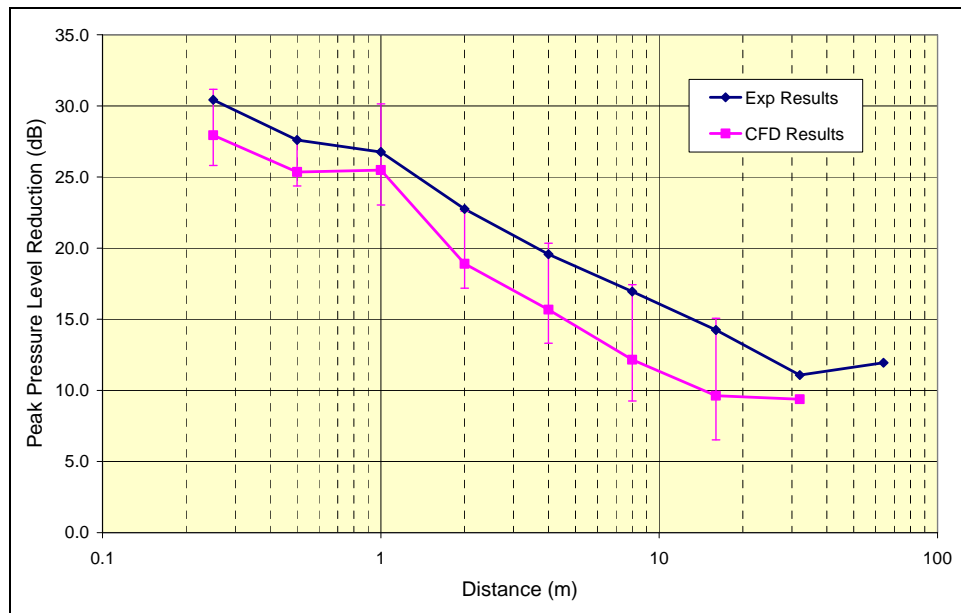

Figure 15. Impulse input peak pressure reduction.

It is likely necessary to model the ear canal in order to improve the results. One may not need the actual shape of the ear canal; the diameter and length might be adequate to ensure the recording location in the CFD is the same distance from the CAE acoustic element as the tympanic membrane in the human ear. Figure 16 shows the input impulse pressure (left scale) and the comparison of the response pressure for the experiment and CFD (right scale) for the 1-m case. Data for the other impulse source distances were similar. The CFD values show a quicker rise and a "ringing" effect. The faster rise time is due to the recording probe location being closer to the CAE element. The ringing effect is due to the reflection of the pressure wave from the outlet of the extended chamber region. This outlet is not present in the experimental case and is an artifact of the simulation setup. Modeling the proper length and volume of the ear canal should improve these results. Wave reflection is also present in the experimental response pressure but is damped more than in the simulation.
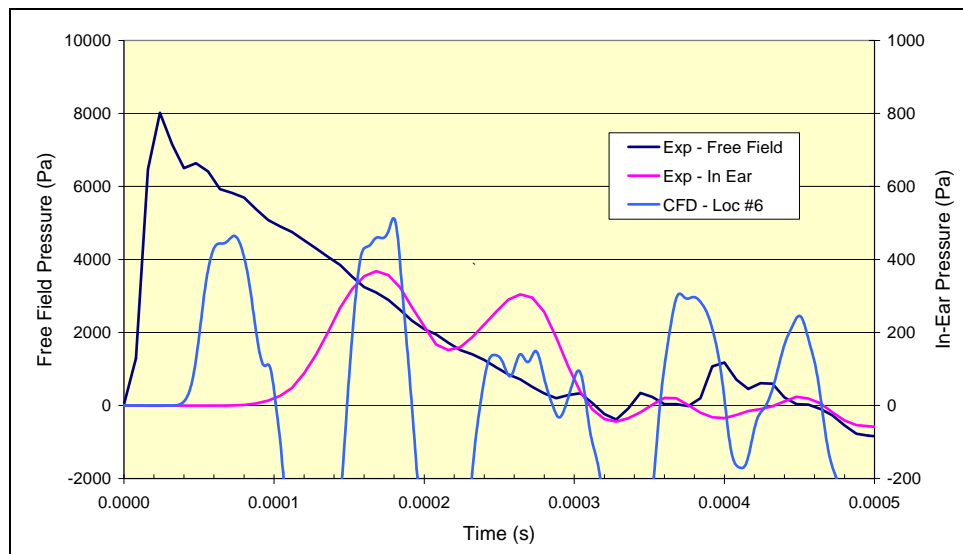

Figure 16. Comparison of experimental and predicted pressure response; M4 rifle at 1 m.

4. Conclusions

The experimental REAT measurements compared very well with the design specifications for the CAE. The experimental continuous noise measurements showed higher than desired attenuation in the 1- to 4-kHz range. The experimental impulse tests provided a good set of data to validate the CFD predictions. CFD predictions of the continuous noise input cases underpredicted the attenuation at the higher frequencies, but the general shape of the response curve was predicted well above 1000 Hz. Using a pink noise input to match the experimental data should improve these results.

Predicted values for impulse noise attenuation were good, to within 15% of the experimental values. These results should improve by adjusting the modeling of the downstream passageway to the impulse receiving element. Modeling the actual ear canal is not trivial; however, it can be implemented with a small increase in computational resources. It is believed that, with further refinement, the CFD modeling may be used to evaluate the effectiveness of level-dependent HPDs and provide direction for improvements to the design of these devices.

5. References

1. Berger, E. H. Using KEMAR to Measure Hearing Protector Attenuation: When it Works, and When it Doesn't. In *Proceedings of Inter-Noise 92*; Daigle, G. A., Stinson, M. R., Eds.; Noise Control Foundation: Poughkeepsie, NY, 1992; pp 273–278.

2. Berger, E. H. Preferred Methods for Measuring Hearing Protector Attenuation. *Proceedings of the 2005 Congress and Exposition on Noise Control Engineering*; Rio De Janeiro, Brazil, 7–10 August 2005. http://www.e-a-r.com/pdf/hearingcons/T05-01_I-NOISEMeth.pdf (downloaded 16 March 2007).

3. ANSI S12.6-1997 (R2002). *Methods for Measuring the Real-Ear Attenuation of Hearing Protectors* **1997**.

4. Smith, S. W. *The Scientist and Engineer's Guide to Digital Signal Processing*, 2nd ed.; California Technical Publishing: San Diego, CA, 1999.

5. *FLUENT v6.3 User's Guide*; Fluent, Inc.: Lebanon, NH, 2006.

6. Russel, D. A. Acoustic High-Pass, Low-Pass, and Band-Stop Filters. http://www.kettering.edu/~drussell/GMI-Acoustics/Filters.html (accessed 21 June 2005).

7. Middelberg, J. M.; Barber, T. J.; Leong, S. S.; Byrne, K. P.; Leonardi, E. Computational Fluid Dynamics Analysis of the Acoustic Performance of Various Simple Expansion Chamber Mufflers. *Proceedings of Acoustics 2007*, Gold Coast, Australia, 3–5 November 2004.

8. Selamet, A.; Ji, Z. L. Acoustic Attenuation Performance of Circular Expansion Chambers With Extended Inlet/Outlet. *Journal of Sound and Vibration* **1999**, *223* (2), 197–212.

9. Kinsler, L. E.; Frey, A. R.; Coppens, A. B.; Sanders, J. V. *Fundamentals of Acoustics*, 4th ed.; John Wiley & Sons: New York, 2000.

10. E-A-R, Aearo Company. http://www.aearo.com/pdf/CombatArms_SS_Final.pdf (accessed 19 October 2007).

NO. OF
COPIES ORGANIZATION

   1   DEFENSE TECHNICAL
  (PDF   INFORMATION CTR
  only)   DTIC OCA
          8725 JOHN J KINGMAN RD
          STE 0944
          FORT BELVOIR VA 22060-6218

   1   US ARMY RSRCH DEV &
          ENGRG CMD
          SYSTEMS OF SYSTEMS
          INTEGRATION
          AMSRD SS T
          6000 6TH ST STE 100
          FORT BELVOIR VA 22060-5608

   1   DIRECTOR
          US ARMY RESEARCH LAB
          IMNE ALC IMS
          2800 POWDER MILL RD
          ADELPHI MD 20783-1197

   1   DIRECTOR
          US ARMY RESEARCH LAB
          AMSRD ARL CI OK TL
          2800 POWDER MILL RD
          ADELPHI MD 20783-1197

   1   DIRECTOR
          US ARMY RESEARCH LAB
          AMSRD ARL CI OK T
          2800 POWDER MILL RD
          ADELPHI MD 20783-1197

          ABERDEEN PROVING GROUND

   1   DIR USARL
          AMSRD ARL CI OK TP (BLDG 4600)

  2   ANSYS INC
        CENTERRA RESOURSE PARK
        R HARWOOD
        S WIROGO
        10 CAVENDISH CT
        LEBANON NH 03766-1442

ABERDEEN PROVING GROUND

 20   DIR USARL
        AMSRD ARL HR
          P DEITZ
          T LETOWSKI
        AMSRD ARL HR SD
          B AMREIN
          M BINSEEL
          J KALB
        AMSRD ARL HR M
          F PARAGALLO
        AMSRD ARL WM
          S KARNA
          J MCCAULEY
          J SMITH
          T WRIGHT
        AMSRD ARL WM B
          J NEWILL
          M ZOLTOSKI
        AMSRD ARL WM BA
          D LYON
        AMSRD ARL WM BC
          P WEINACHT
          J DESPIRITO
          K HEAVEY
          S SILTON
        AMSRD ARL WM BD
          B FORCH
        AMSRD ARL WM BF
          W OBERLE
        AMSRD ARL VT UV
          M BUNDY

INTENTIONALLY LEFT BLANK.